Extreme Mechanics Letters 68 (2024) 102147

Contents lists available at ScienceDirect

Extreme Mechanics Letters

journal homepage: www.elsevier.com/locate/eml

Scaling between elasticity and topological genus for random network nanomaterials

Seoyun Sohn [a], Claudia Richert [a], Shan Shi [b,a,*], Jörg Weissmüller [c,a], Norbert Huber [a,c]

[a] Institute of Materials Mechanics, Helmholtz-Zentrum Hereon, Geesthacht, Germany
[b] Research Group of Integrated Metallic Nanomaterials Systems, Hamburg University of Technology, Hamburg, Germany
[c] Institute of Materials Physics and Technology, Hamburg University of Technology, Hamburg, Germany

ARTICLE INFO

Keywords:
Nanoporous gold
Scaling laws
Network materials
Topological genus
Elasticity
Finite-element modeling

ABSTRACT

We explore the hypothesis that the variation of the effective, macroscopic Young's modulus, E_{eff}, of a random network material with its scaled topological genus, g, and with the solid fraction, φ, can be decomposed into the product of g- and φ-dependent functions. Based on findings for nanoporous gold, supplemented by the Gibson–Ashby scaling law for E_{eff}, we argue that both functions are quadratic in bending-dominated structures. We present finite-element-modeling results for E_{eff} of coarsened microstructures, in which g and φ are decoupled. These results support the quadratic forms.

1. Introduction

Materials with random network microstructures have numerous manifestations. In biology they form the cytoskeleton of cells and the collagen in connective tissue, and in the inanimate world they can take the form of scaffolds at the molecular scale, as in rubber or gels, to micron- or millimeter scales as in polymer consumer products and metallic low-density open-cell foams [1–4]. Often, one of their key functions is to bear load. In this respect, network nanomaterials are attractive, since the strengthening that comes with reducing the size of the network struts may partly compensate for the weakening due to the low solid fraction [5–9]. Thus, network nanomaterials may combine high mass-specific strength or stiffness with low density [9–13]. Ordered network nanomaterials can be made in the form of 3D manufactured periodic lattices with unit cells engineered for optimum performance [9–12]. Cellular materials can also be designed as shell structures of particularly low density, allocating the load-bearing function to the interfacial region between two void phases [14–16]. Yet, nanoscale structuring also brings a dramatic increase in the number of structural elements per volume, favoring preparation by nature's self organization processes over controlled 3D manufacturing [13]. The microstructure is then again random, as in the wider class of materials addressed at the outset.

Nanoporous gold (NPG) [17] is a network nanomaterial that can be prepared, highly reproducibly, as uniform macroscopic bodies that can be mechanically tested with reliable macroscale schemes [18–22]. Its microstructure is well represented [23] by the leveled-wave model [24], which also underlies the random microstructures of a wider range of materials, including spinodally decomposed solid solutions, porous glasses such as vycor, as well as some microemulsions and polymer blends [25–30]. This qualifies NPG as a model material for nanoscale random networks in general, and specifically for studies of their mechanics. During the past decade, experiments have established a consistent picture of NPG's mechanical behavior [8].

Understanding the mechanics of random networks, such as NPG, requires that the relevant statistical microstructure parameters are identified and their impact on the mechanics analyzed. The solid volume fraction, φ, is a central parameter in related predictive theory. That parameter also underlies scaling laws for the mechanics of crystalline networks that are being considered in the context of NPG [31,32]. In addition, recent research advertises the network connectivity as an additional microstructural metric controlling the mechanics of NPG [21,33–37]. Yet, the scaling between the effective Young's modulus, E_{eff}, as an elementary mechanical materials parameter and the connectivity in random network materials remains to be established.

Here, we explore the just-mentioned connection, and we condense the observations in a scaling law. Our study exploits the existing database, from experiment and simulation, on E_{eff} of the random network material NPG, and it adds novel simulation data for leveled-wave-like random networks with different connectivity.

* Corresponding author at: Research Group of Integrated Metallic Nanomaterials Systems, Hamburg University of Technology, Hamburg, Germany.
E-mail address: shan.shi@tuhh.de (S. Shi).

https://doi.org/10.1016/j.eml.2024.102147
Received 6 September 2023; Received in revised form 19 February 2024; Accepted 3 March 2024
Available online 6 March 2024

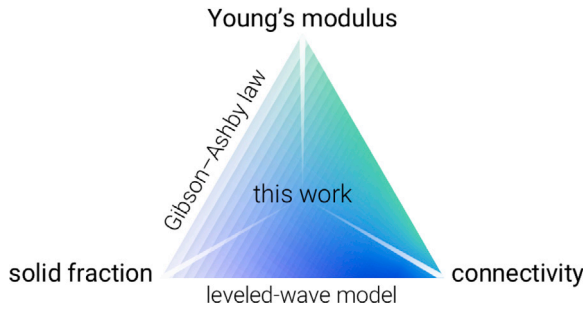

Fig. 1. A pictorial summary of previous works [37,38] and this work. The Gibson–Ashby scaling law is valid only for a constant connectivity case, as visualized by the lines parallel to the upper left edge of the triangle. The leveled-wave model assumes a fixed analytical relation between solid fraction and connectivity. This work reports a generalized scaling relation between the three parameters — Young's modulus, solid fraction, and connectivity.

2. Theory

Fig. 1 shows a pictorial summary of previous works [37,38] and this work on the scaling law for the effective macroscopic Young's modulus of random network materials. For many classes of materials with network microstructures, φ can be varied while the connectivity of the underlying skeleton remains constant. For small φ and bending-dominated networks, Young's modulus then follows the Gibson–Ashby scaling law [38,39]

$$E_{\mathrm{eff}} = \varphi^2 E_0 \,, \tag{1}$$

with E_0 Young's modulus of the base material. The Gibson–Ashby law of Eq. (1) has been derived for a periodic lattice of unit cells consisting of struts connected in nodes. The solid fraction is varied through the strut aspect ratio while maintaining the architecture and specifically the connectivity invariant. Systematic deviations from Eq. (1) in NPG have been linked to variations in the connectivity with φ.

An exemplary background for our discussion is provided by the leveled-wave model (see above). Motivated by the microstructure evolution during the diffusive spontaneous decomposition of thermodynamically unstable binary solutions (spinodal decomposition), the leveled-wave microstructure is generated by superimposing plane waves of random wave vector orientation and with random phase shifts but with identical wavelength, λ, and then applying a level-cut for binarizing with the requested φ [24]. As leveled-wave structures of different λ are self-similar, the model has φ as the only morphology-changing parameter. The connectivity is uniquely determined by φ and varies strongly with that parameter. In experiments, φ is typically measured, and that parameter forms the microstructure variable in scaling laws. Thus, the comparison between leveled-wave microstructures and experiment involves no free parameters. It is therefore remarkable that the model's stiffness and strength agree closely with experiment on as-prepared NPG [13,37].

The leveled-wave model exhibits a percolation-to-cluster transition at solid fraction $\varphi_{\mathrm{p}} \approx 0.159$ [37]. Whereas the stiffness of $\varphi \approx 1/2$ leveled-wave manifestations is similar to that of periodic network structures of same φ, manifestations with $\varphi < \varphi_{\mathrm{p}}$ contain no contiguous load bearing paths and so have vanishing stiffness.

The topological genus, G, measures the connectivity of a body. G represents the maximum number of connections that can be cut while still leaving the body contiguous. For instance, the genus values of a sphere, a doughnut, and a brezel are 0, 1, and 2, respectively. For a network with a given microstructure, the extensive property G scales with the volume, V, since structures with twice the volume will contain twice the number of connections. Furthermore, structures with the same volume but half the microstructural length scale will contain eightfold as many microstructural elements and, hence, eightfold as many connections. Thus, G scales inversely with the cube of the characteristic microstructural length scale, L. The scaled genus, g, is introduced as a volume- and scale-independent characteristics of the microstructural morphology; it is defined as the mean number of connections in an elemental building block, of volume L^3, of the microstructure [35,40–42],

$$g = \frac{GL^3}{V} \,. \tag{2}$$

Here, we adopt a convention for L that connects g uniquely to the skeleton topology, independent of φ. This convention identifies L with the characteristic spacing, $\tilde{L}$, between microstructural elements, as embodied in the first maximum of the autocorrelation function or, equivalently, in the first maximum in the interference function [37]. For the example of the leveled-wave model, it also implies $\tilde{L} = \alpha\lambda$ with $\alpha = 1.23$.

The scaled genus of the leveled-wave model varies with φ according to [37]

$$g = \frac{2\pi\alpha^3}{3\sqrt{3}} \left(1 - \xi^2\right) \exp\left(-\frac{\xi^2}{2}\right)$$
$$\xi = \sqrt{2}\,\mathrm{erf}^{-1}\left(2\varphi - 1\right) \,. \tag{3}$$

The prediction of Eq. (3) for $g(\varphi)$ is shown in Fig S1 of the Supporting Information (SI). Note the complete loss of connectivity at the percolation threshold.

In NPG, $\tilde{L}$ can be tuned by deliberate coarsening. Annealing accelerates the surface diffusion, and this lets the microstructure evolve in such a way that the net area of surface and, hence, the net excess surface energy is decreased, with a concomitant increase in $\tilde{L}$. That process can entail a strong decrease in E_{eff}. While atomistic simulations using embedded-atom interatomic potentials suggest a noticeable size-dependence of the effective elastic behavior of metal nanostructures [43,44], more realistic investigations based on density functional theory establish that an inherent size-dependent elasticity can be expected in individual struts only for ligament sizes well below 10 nm [45]. Thus, the experimentally observed decrease in E_{eff} of NPG indicates a loss in connectivity [33,34]. Even in the as-prepared state of NPG, a strong and systematic deviation of $E_{\mathrm{eff}}(\varphi)$ from the Gibson–Ashby behavior has been linked to variations in the connectivity: as NPG's density is reduced, g will systematically drop (as implied by Eq. (3)), with a concomitant drop in E_{eff} [37].

A convenient hypothesis states that the joint impact of solid fraction and of connectivity on E_{eff} of random network structures can be separated in a product [36,41],

$$E_{\mathrm{eff}} = f_{\mathrm{g}}(g) f_{\varphi}(\varphi) E_0 \tag{4}$$

with f_{g} and f_{φ} dimensionless scaling functions.

Eq. (1) provides a special case of Eq. (4) for constant g. Its suggestion that $f_{\varphi} \propto \varphi^2$ reflects the mechanics of network structures in the limit of long thin struts, where φ is low and the elastic deformation is bending-dominated. In terms of the strut aspect ratio, r (diameter over length), one finds that $\varphi \propto r^2$ and that the bending moment M, which determines the stiffness, scales as $M \propto r^4 E_0$. This immediately leads to the quadratic f_{φ} [38] and, hence, to the special form of Eq. (4) for bending-dominated network structures,

$$E_{\mathrm{eff}} = f_{\mathrm{g}}(g) \varphi^2 E_0 \,. \tag{5}$$

The argument holds independent of the detailed topological architecture (number and arrangement of struts in the representative local building block) of the network and, therefore, also independent of its connectivity.

Mangipudi et al. [41] have computed E_{eff} for a set of model microstructures by finite-element-modeling (FEM). Exploiting Eq. (5), they suggest a linear form, $f_{\mathrm{g}} \propto g$. Their set of model structures contains both, periodic and random networks. In that context it is significant

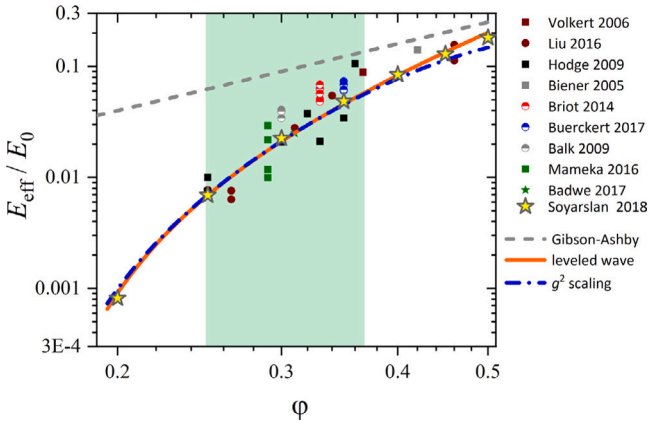

Fig. 2. Normalized effective Young's modulus $E_{\rm eff}/E_0$ versus solid fraction φ. Dashed line, Gibson–Ashby scaling law. Solid line, modified Roberts–Garboczi law, Eq. (7). Dash-dotted line, genus-dependent scaling law, Eq. (8). Symbols, experimental results for as-prepared nanoporous gold reported by [6,19,21,33,47–51] and FEM data for the leveled-wave model [37].

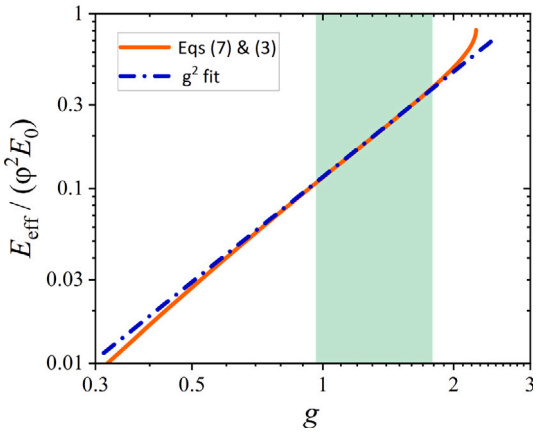

Fig. 3. Topology-dependent scaling in the leveled-wave model. The function $E_{\rm eff}/(\varphi^2 E_0)$, with Eq. (7) for $E_{\rm eff}$, represents the elastic leading constant f_g. Solid line shows parametric graph of $f_g(\varphi)$ versus the solid-fraction- (φ-) dependent topological genus $g(\varphi)$ of Eq. (3) in the region $\varphi = 0.2-0.5$. Shaded: experimental region of interest as marked in Fig. 2. Dashed: fit with a quadratic g-dependence in that region.

that $E_{\rm eff}$ is not uniquely determined by φ even for periodic network structures with a given unit cell and identical g. For instance, random displacements of the nodes can bring a substantial decrease in $E_{\rm eff}$ [31], and the morphology of the struts requires consideration [46]. Those observations are not immediately compatible with deriving scaling laws – such as that of Mangipudi et al. – by analysis of a set combining ordered periodic with random structures.

Focusing on NPG, Jin and coworkers have introduced and experimentally substantiated the notion of an effective load-bearing solid fraction, $\varphi_{\rm eff}$, which can replace φ in Eq. (1). Their $\varphi_{\rm eff}$ counts only the load-bearing regions of the solid, ignoring the volume of "broken" struts that do not contribute to the mechanics [33,34]. Their work does not address the topological genus and so leaves open how $\varphi_{\rm eff}$ relates to g. Yet, in their spirit and in agreement with [36], one may assume a linear scaling between the two quantities — starting out from a well-connected reference structure, every broken strut reduces g and $\varphi_{\rm eff}$ in the same proportion. In other words,

$$\varphi_{\rm eff}(g,\varphi) = \frac{g}{g_0}\varphi\,. \tag{6}$$

with g_0 a constant that depends on the geometry of the reference structure. In view of Eq. (1), Eq. (6) would imply that the connectivity-elasticity law might be quadratic, as opposed to the linear relation suggested in [41].

For the leveled-wave model and $\varphi \ll 0.5$, a modification,

$$E_{\rm eff} = C_{\rm R}\left(\frac{\varphi-\varphi_{\rm p}}{1-\varphi_{\rm p}}\right)^m E_0\,, \tag{7}$$

of the Roberts–Garboczi scaling law for random networks [28] has been found to agree well with experimental data for as-prepared NPG and with numerical results for $E_{\rm eff}$ of the leveled-wave model [37]. The adjustable parameters in Eq. (7) there take $C_{\rm R} = 2.03$ and $m = 2.56$.

Fig. 2 shows Eq. (7), superimposed to experimental literature data for as-prepared NPG [6,19,21,33,47–51] and to FEM data for the leveled-wave model [37]. The strong deviation from the Gibson–Ashby law at low φ is a signature of the loss of connectivity as the percolation threshold is approached. Other scaling laws add a term linear in φ to the quadratic dependence of the Gibson–Ashby law [32,52], thereby accounting for stretching- as opposed to bending-dominated deformation at higher solid fractions. Such laws have not been tested against similarly large data sets as Eq. (7), and our inspection (dotted line in Fig S2) indicates that they fail to reproduce the low-φ behavior of experiment and numerical simulation for the random-network material NPG.

As mentioned above, the drop in $E_{\rm eff}$ upon coarsening of NPG [21,33,34] suggests a loss in connectivity. Yet, data for g is not available for those experiments. Studies by experimental 3D tomographic reconstruction [41,42,53] explore how g evolves upon coarsening. Those studies conclude on self-similar coarsening with essentially invariant g. Kinetic Monte Carlo (KMC) simulation suggests $\varphi = 0.3$ as a threshold, with self-similar coarsening at larger φ and loss of connectivity at lesser φ [54]. Data exploring $E_{\rm eff}$ during a systematic variation of g in NPG, which could reveal the topology-dependence of the elasticity, has not been reported.

Our approach to a genus-dependent scaling law for NPG starts out with matching f_g in Eq. (5) to the leveled-wave model. We may here compute the values of f_g as $E_{\rm eff}/(\varphi^2 E_0)$, using Eq. (7) for $E_{\rm eff}$. Together with Eq. (3) for $g(\varphi)$, the aforementioned expression for $f_g(\varphi)$ forms an implicit representation of the f_g versus g relation with φ as a parameter. This representation is shown as the solid line in Fig. 3.

Practically all experimental studies of NPG have φ in the range $0.2 - 0.45$ and, as exemplified by our Fig. 2, their majority is in the even smaller interval $0.25 - 0.37$, shaded in the figure. In Fig. 3, a linear fit (blue solid line) on logarithmic scales in the same interval (shaded) obtains $f_g = (g/2.88)^{2.04}$. This supports our hypothesis of an essentially quadratic relation between f_g and g. Superimposed to the exact parametric plot, Fig. 3 shows a best fit with the quadratic law (dashed line), again for the same, experimentally most relevant, interval. In the region of interest, the fit, $f_g = (g/2.93)^2$, is seen to provide an excellent approximation to the parametric graph. Applying the fit back to Eq. (5), the new scaling law reads

$$E_{\rm eff} = \left(\frac{g}{g_0}\right)^2 \varphi^2 E_0 \tag{8}$$

with $g_0 = 2.93$.

Fig. 2 shows the genus-dependent scaling law of Eq. (8) (using Eq. (3) for g of the leveled-wave model) superimposed to the literature data and to the scaling law of Eq. (7). The agreement with experiment is apparent.

One immediately sees that the new scaling law of Eq. (8) can be interpreted as a modified Gibson–Ashby law, with φ replaced by the effective solid fraction, $\varphi_{\rm eff}$, of Eq. (6), in other words,

$$E_{\rm eff} = \varphi_{\rm eff}^2(g,\varphi) E_0\,. \tag{9}$$

This confirms our speculation, based on the notion by Liu et al. [33] of an effective load-bearing solid fraction. For comparison, Fig S2 in the SI inspects the linear g-scaling suggested in [41]. We find that scaling hypothesis not to provide a satisfactory fit to the data in Fig. 2.

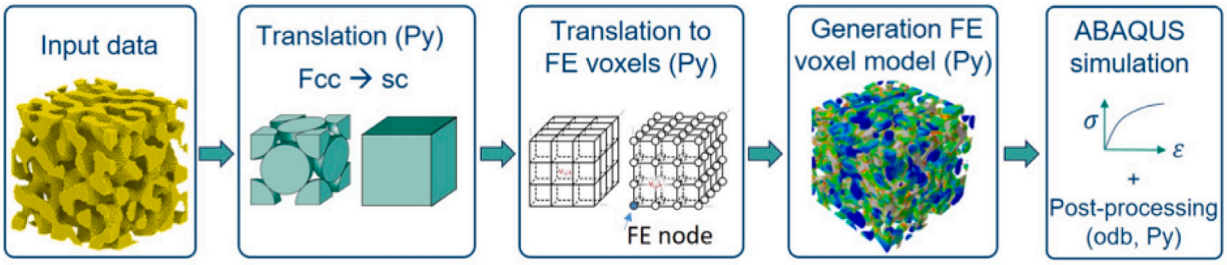

Fig. 4. Workflow for the creation and simulation of an FE voxel model for leveled-wave structures. The input data for coarsened leveled wave structures is from the dataset in [55]. A translation from a face-centered-cubic (fcc) to simple-cubic (sc) grid allows creating cubic FE elements representing the individual solid voxels. Colors in the generated FE voxel model indicate the von Mises stress distribution as result of the numerical simulation of the model during compression in vertical direction. Homogenization delivers the macroscopic stress–strain behavior, from which E_{eff} is derived in a postprocessing step. (For interpretation of the references to color in this figure legend, the reader is referred to the web version of this article.)

3. Computational results for networks of reduced connectivity

So far, our analysis of the genus-dependent scaling rests exclusively on the leveled-wave model, where φ and g are inextricably coupled (Eqs. (3) and (7)). The constraint $g = g(\varphi)$ implies that the separation into the functions f_g and f_φ is not forceful and requires independent support, conveniently in the form of data for networks with same φ but different g.

One approach to varying the connectivity of networks is the random cutting of the struts of a periodic lattice. A universal relation, independent of the coordination number of the perfect reference lattice, links E_{eff} to a suitably normalized total cut fraction or a suitably normalized scaled genus [36]. Yet, specifying a fraction of cuts or, alternatively, normalizing the scaled genus to the correct reference volume (correct choice of L in Eq. (2) for the reference structure), requires that a perfect reference structure is identified in the first place. That task is not obvious for random network structures, and specifically in experiment. Here, we exploit that coarsening of leveled-wave like structures, a process that is driven by curvature-driven surface diffusion, can change g while leaving φ sensibly constant.

A data set based on KMC simulations and exploring the change in connectivity of NPG during coarsening is reported in [54,55]. The simulation accounts for surface excess energy as the driving force and for surface diffusion as the atomistic mechanism of microstructure evolution. That data provides samples with φ and g decoupled. We have imported the 3D representations from that work into FEM simulations and computed the E_{eff} following the workflow shown in Fig. 4. To create an FE voxel model, the simple cubic cell of the fcc structure is mapped onto one voxel. For the 200 lattice unit cells per simulation box edge, this results in a FE model of 200 × 200 × 200 voxels. The cut-off for the number of active atoms per cell was chosen such that the resulting solid fraction in the FE voxel model was closest to the solid fraction of the original fcc structure. Because of the discretization error, deviations in the resulting solid fraction of the FE voxel model were between −5% and 8%. For further improvement, partial voxels were introduced that were assigned with a reduced Young's modulus, weighted with the filling fraction of the corresponding voxel. Consequently, values of φ and g could be adopted from [54,55] for the following analysis. The material parameters of the solid gold phase were $E_0 = 79$ GPa and Poisson's ratio $\nu = 0.42$, following [37]. The results of the numerical simulation are compiled in tabular form as an SI data sheet; see description in Sec. S6.

Exemplary von Mises stress fields from our simulations are shown in Fig. 5. Blue designates stress-free regions. These regions are typically disconnected from the main load-bearing cluster. They can be seen to become more frequent in later stages of coarsening, specifically for structures with low φ. This illustrates the gradual disconnection upon coarsening.

For all structures of the coarsening simulation, Fig. 6 shows E_{eff}, normalized to the Gibson–Ashby prediction $\varphi^2 E_0$, versus g. Thus, as

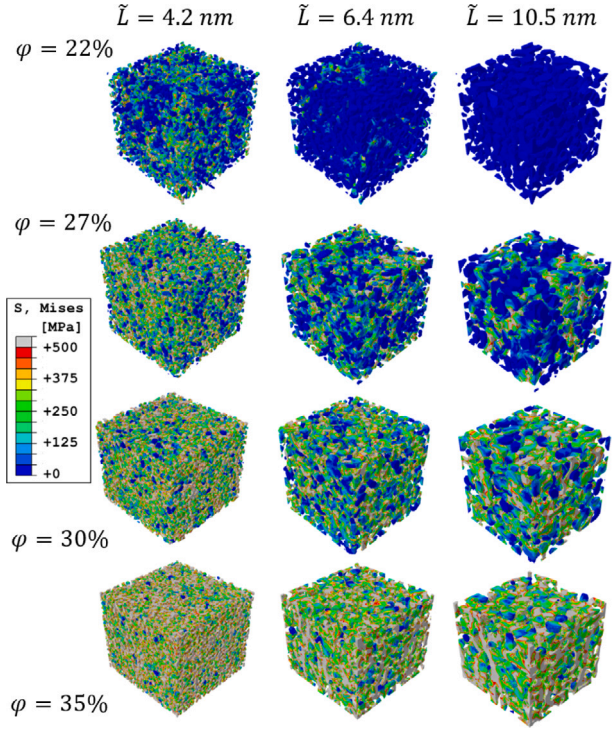

Fig. 5. Load distribution in leveled-wave type structures visualized via elastic–plastic compression to 10% strain and its evolution during coarsening. Finite-element method results for local von Mises stress (legend). Rows: four samples of different solid fraction φ. Columns: as-generated and coarsened to characteristic spacing $\tilde{L}$ (legend). (For interpretation of the references to color in this figure legend, the reader is referred to the web version of this article.)

in Fig. 3, the ordinate displays f_g. Each symbol type in the figure represents a (numerical) sample with a given φ. Groups of symbols for each sample are connected by lines, following that sample's evolution during the coarsening. The initial state is marked × for each sample. By construction of the KMC simulation, each sample has constant φ during the entire coarsening.

Most samples in Fig. 6 exhibit an initial increase in g. This evolution does not imply new connections. Instead, it results from an error in computing $\tilde{L}$ of the as-generated structure. The error propagates into the computation of g by Eq. (2) and lets g initially be underestimated by up to ∼ 40%. The problem is explained in [54] and the underlying issues are collected in the SI.

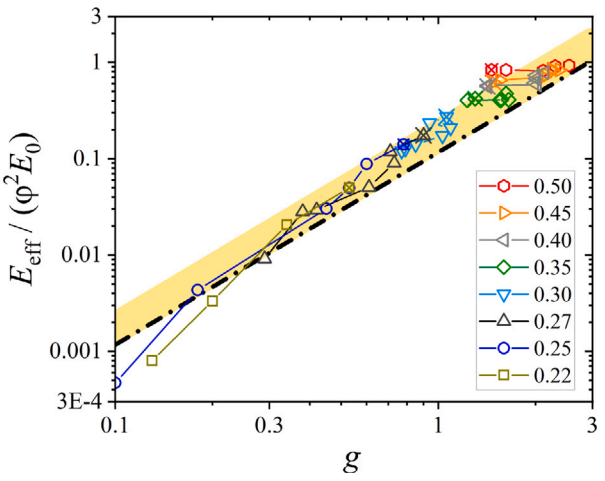

Fig. 6. Analysis of connectivity scaling for effective Young's modulus, E_{eff}, of computer-generated structures with reduced connectivity. E_{eff} (normalized to the Gibson–Ashby prediction $\varphi^2 E_0$) is shown versus scaled genus, g. Data points: results from modeling of coarsened nanoporous gold. For solid fraction φ see legend. Colored lines connect data points of structures with common φ, in sequence of increasing coarsening time. Initial structures are marked ×. Note log–log scaling. Dashed line: Eq. (8), with $g_0 = 2.93$ for the leveled-wave model. Shaded: confidence band with $g_0 = 2.40 \pm 0.50$. (For interpretation of the references to color in this figure legend, the reader is referred to the web version of this article.)

During the later stages of the coarsening, Fig. 6 shows the samples behaving quite differently. Samples with high φ experience little change in E_{eff} during coarsening. By contrast, E_{eff} of the samples with low φ drops significantly as the coarsening proceeds, along with a drop in g. This may be understood as the signature of the above-mentioned loss in connectivity during coarsening of low-φ random microstructures.

Setting aside the artifact of the initial decrease in g, the central feature in Fig. 6 is that E_{eff} decreases with g in agreement with the g^2 scaling law of Eq. (8) (dashed line). In other words, the FEM results for microstructures in which g varies independently of φ support the proposed scaling law.

The shaded band in Fig. 6 contains all data points but ignoring the initial ones (for the reason outlined above) and the ones at extremely small g, where the stiffness starts to fall significantly below the g^2 scaling. The band represents $g_0 = 2.40 \pm 0.50$. It underlines that the data for the sample with varying connectivity is compatible with our suggested scaling law, yet with g_0 about 20% smaller than what was found for the as-prepared, non-coarsened leveled-wave structures of [37].

As is explained in the SI, different values of the E_{eff} in the two FEM studies (this work and [37]) may reflect differences in how the microstructure was discretized when setting up the models for the numerical analysis. In spite of the different g_0, our observations on the two different data sets are likely compatible with the identical underlying scaling law.

One may ask about the physics behind the numerical value of g_0. The largest g of leveled-wave like random network structures is 2.25 (Eq. (3) with $\varphi = 1/2$) and this is within the confidence band. Our findings are thus compatible with the notion of the NPG and leveled-wave structures as derived from an "ideal" random network simply by cutting connections. That ideal network would have $g = g_0 = 2.25$.

4. Conclusions

The success [39] of the Gibson–Ashby scaling law for stochastic or periodic open-cell microstructures with widely different geometries (and, apparently, similar connectivity) shows that mechanics and microstructural geometry can be coupled by simple scaling relations. In that instance, the governing microstructural metric is the solid fraction, φ.

Our results unraveled a separate scaling, namely between the mechanics and the network connectivity as measured by the scaled topological genus, g. At constant φ, the effective Young's modulus scales with g^2 as embodied in Eq. (8) as the central result of this work. As this scaling derives from leveled-wave-like structures, it is a priori restricted to a specific class of morphologies. That being said, the leveled-wave model has been established to represent a significant range of materials with random bicontinuous microstructures, supporting the relevance of the new scaling law.

The apparent commonality in the architecture of different classes of porous and random network materials may be understood as a consequence of similarities in the driving forces and transport mechanisms of the microstructure evolution. The prototypical processes behind leveled-wave-like structures are early-stage spinodal decomposition and later-stage spinodal coarsening, in which surface- or bulk-diffusion act most efficiently at small scale while interfacial free energy minimization favors large scales. The same mechanisms also control the breaking of network struts by Plateau–Rayleigh instabilities. Interfacial energy is generally relevant for porous materials, and diffusive transport is often a prerequisite for microstructure evolution during their formation. This supports the leveled-wave microstructure as a physically motivated model.

In architected periodic lattices, any microstructural descriptor–including the number and relative angle of struts meeting in a node [9,11,12,56] as well as axial [57–59] and cross-sectional [60] shape factors of the struts — can, in principle, be freely engineered. The accessible parameter space for microstructure design is thus drastically wider than what is explored by nature's spinodal-like microstructure evolution processes, and the conclusions of the present work cannot forcefully be transferred to architected structures from the more general parameter space. Indeed, a study of the elasticity of lattice networks with idealized cylindrical struts that are randomly cut [36] does not support a simple power-law relation between Young's modulus and scaled genus (see SI, Sec S5). Yet, that study does support the present findings by exposing the scaled-genus dependence of the elasticity as decoupled from other factors, as in our Eq. (4).

In respect to the indications of universal scaling within individual families of network structures, recall that the simplest argument leading to the g^2 scaling is based quite fundamentally on the load-bearing solid fraction. That concept might hold for more general types of random microstructures, beyond the leveled-wave-like ones. This may be seen as an incentive for future checks of the link between connectivity and mechanics in a wider variety of structures.

CRediT authorship contribution statement

Seoyun Sohn: Writing – review & editing, Writing – original draft, Investigation, Formal analysis. **Claudia Richert:** Writing – review & editing, Methodology, Investigation, Formal analysis. **Shan Shi:** Writing – review & editing, Writing – original draft, Supervision, Formal analysis, Conceptualization. **Jörg Weissmüller:** Writing – review & editing, Writing – original draft, Supervision, Funding acquisition, Formal analysis, Conceptualization. **Norbert Huber:** Writing – review & editing, Writing – original draft, Supervision, Funding acquisition, Formal analysis, Conceptualization.

Declaration of competing interest

The authors declare the following financial interests/personal relationships which may be considered as potential competing interests: Seoyun Sohn, Claudia Richert, Shan Shi, Joerg Weissmueller and Norbert Huber reports financial support was provided by German Research Foundation.

Data availability

Data will be made available on request.

Acknowledgments

This work was supported by Deutsche Forschungsgemeinschaft (DFG, German Research Foundation) through the Collaborative Research Initiative SFB 986 “Tailor-Made Multi-Scale Materials Systems: M3”, Project-ID 192346071.

Appendix A. Supplementary data

Supplementary material related to this article can be found online at https://doi.org/10.1016/j.eml.2024.102147.

References

[1] L.J. Gibson, Mechanical behavior of metallic foams, Annu. Rev. Mater. Sci. 30 (1) (2000) 191–227.
[2] W.-Y. Jang, A.M. Kraynik, S. Kyriakides, On the microstructure of open-cell foams and its effect on elastic properties, Int. J. Solids Struct. 45 (7) (2008) 1845–1875.
[3] R.C. Picu, Mechanics of random fiber networks—a review, Soft Matter 7 (15) (2011) 6768–6785.
[4] R.H. Pritchard, Y.Y. Shery Huang, E.M. Terentjev, Mechanics of biological networks: from the cell cytoskeleton to connective tissue, Soft Matter 10 (12) (2014) 1864–1884.
[5] J. Biener, A.M. Hodge, J.R. Hayes, C.A. Volkert, L.A. Zepeda-Ruiz, A.V. Hamza, F.F. Abraham, Size effects on the mechanical behavior of nanoporous Au, Nano Lett. 6 (10) (2006) 2379–2382.
[6] C.A. Volkert, E.T. Lilleodden, D. Kramer, J. Weissmuller, Approaching the theoretical strength in nanoporous Au, Appl. Phys. Lett. 89 (6) (2006).
[7] A.M. Hodge, J. Biener, J.R. Hayes, P.M. Bythrow, C.A. Volkert, A.V. Hamza, Scaling equation for yield strength of nanoporous open-cell foams, Acta Mater. 55 (4) (2007) 1343–1349.
[8] H.-J. Jin, J. Weissmüller, D. Farkas, Mechanical response of nanoporous metals: A story of size, surface stress, and severed struts, MRS Bull. 43 (1) (2018) 35–42.
[9] J. Bauer, L.R. Meza, T.A. Schaedler, R. Schwaiger, X. Zheng, L. Valdevit, Nanolattices: an emerging class of mechanical metamaterials, Adv. Mater. 29 (40) (2017) 1701850.
[10] T.A. Schaedler, A.J. Jacobsen, A. Torrents, A.E. Sorensen, J. Lian, J.R. Greer, L. Valdevit, W.B. Carter, Ultralight metallic microlattices, Science 334 (6058) (2011) 962–965.
[11] R. Schwaiger, L.R. Meza, X. Li, The extreme mechanics of micro- and nanoarchitected materials, MRS Bull. 44 (10) (2019) 758–765.
[12] J.R. Greer, V.S. Deshpande, Three-dimensional architected materials and structures: Design, fabrication, and mechanical behavior, MRS Bull. 44 (10) (2019) 750–757.
[13] S. Shi, Y. Li, B.-N. Ngo-Dinh, J. Markmann, J. Weissmüller, Scaling behavior of stiffness and strength of hierarchical network nanomaterials, Science 371 (6533) (2021) 1026.
[14] A. Guell Izard, J. Bauer, C. Crook, V. Turlo, L. Valdevit, Ultrahigh energy absorption multifunctional spinodal nanoarchitectures, Small 15 (45) (2019) 1903834.
[15] M.N. Lee, A. Mohraz, Bicontinuous macroporous materials from bijel templates, Adv. Mater. 22 (43) (2010) 4836–4841.
[16] M.-T. Hsieh, B. Endo, Y. Zhang, J. Bauer, L. Valdevit, The mechanical response of cellular materials with spinodal topologies, J. Mech. Phys. Solids 125 (2019) 401–419.
[17] J. Erlebacher, M.J. Aziz, A. Karma, N. Dimitrov, K. Sieradzki, Evolution of nanoporosity in dealloying, Nature 410 (6827) (2001) 450–453.
[18] H.J. Jin, L. Kurmanaeva, J. Schmauch, H. Rösner, Y. Ivanisenko, J. Weissmüller, Deforming nanoporous metal: Role of lattice coherency, Acta Mater. 57 (9) (2009) 2665–2672.
[19] N.J. Briot, T. Kennerknecht, C. Eberl, T.J. Balk, Mechanical properties of bulk single crystalline nanoporous gold investigated by millimetre-scale tension and compression testing, Phil. Mag. 94 (8) (2014) 847–866.
[20] N.J. Briot, T.J. Balk, Developing scaling relations for the yield strength of nanoporous gold, Phil. Mag. 95 (27) (2015) 2955–2973.
[21] N. Mameka, K. Wang, J. Markmann, E. Lilleodden, J. Weissmüller, Nanoporous gold—Testing macro-scale samples to probe small-scale mechanical behavior, Mater. Res. Lett. 4 (1) (2016) 27–36.
[22] N. Badwe, X. Chen, K. Sieradzki, Mechanical properties of nanoporous gold in tension, Acta Mater. 129 (2017) 251–258.
[23] G. Wittstock, M. Bäumer, W. Dononelli, T. Klüner, L. Lührs, C. Mahr, L.V. Moskaleva, M. Oezaslan, T. Risse, A. Rosenauer, A. Staubitz, J. Weissmüller, A. Wittstock, Nanoporous gold: From structure evolution to functional properties in catalysis and electrochemistry, Chem. Rev. 123 (10) (2023) 6716–6792.
[24] J.W. Cahn, Phase separation by spinodal decomposition in isotropic systems, J. Chem. Phys. 42 (1) (1965) 93–99.
[25] N.F. Berk, Scattering properties of a model bicontinuous structure with a well defined length scale, Phys. Rev. Lett. 58 (25) (1987) 2718–2721.
[26] M. Teubner, Level surfaces of Gaussian random fields and microemulsions, Europhys. Lett. 14 (5) (1991) 403.
[27] J.C. Li, D.K. Ross, Dynamical scaling for spinodal decomposition - a small-angle neutron scattering study of porous vycor glass with fractal properties, J. Phys.: Condens. Matter 6 (2) (1994) 351–362.
[28] A. Roberts, E.J. Garboczi, Computation of the linear elastic properties of random porous materials with a wide variety of microstructure, Proc. R. Soc. Lond. Ser. A Math. Phys. Eng. Sci. 458 (2021) (2002) 1033–1054.
[29] A.P. Roberts, E.J. Garboczi, Elastic properties of model random three-dimensional open-cell solids, J. Mech. Phys. Solids 50 (1) (2002) 33–55.
[30] C.J. Gommes, Stochastic models of disordered mesoporous materials for small-angle scattering analysis and more, Microporous Mesop. Mater. 257 (2018) 62–78.
[31] N. Huber, R.N. Viswanath, N. Mameka, J. Markmann, J. Weissmüller, Scaling laws of nanoporous metals under uniaxial compression, Acta Mater. 67 (2014) 252–265.
[32] H. Liu, N. Abdolrahim, A modified scaling law for stiffness of nanoporous materials based on gyroid cell model, Int. J. Mech. Sci. 166 (2020) 105223.
[33] L.-Z. Liu, X.-L. Ye, H.-J. Jin, Interpreting anomalous low-strength and low-stiffness of nanoporous gold: Quantification of network connectivity, Acta Mater. 118 (2016) 77–87.
[34] L.-Z. Liu, H.-J. Jin, Scaling equation for the elastic modulus of nanoporous gold with “fixed” network connectivity, Appl. Phys. Lett. 110 (2017) 211902.
[35] E.T. Lilleodden, P.W. Voorhees, On the topological, morphological, and microstructural characterization of nanoporous metals, MRS Bull. 43 (1) (2018) 20–26.
[36] N. Huber, Connections between topology and macroscopic mechanical properties of three-dimensional open-pore materials, Front. Mater. (2018).
[37] C. Soyarslan, S. Bargmann, M. Pradas, J. Weissmüller, 3D stochastic bicontinuous microstructures: Generation, topology and elasticity, Acta Mater. 149 (2018) 326–340.
[38] L.J. Gibson, M.F. Ashby, The mechanics of three-dimensional cellular materials, Proc. R. Soc. Lond. Ser. A Math. Phys. Eng. Sci. 382 (1782) (1982) 43–59.
[39] L.J. Gibson, M.F. Ashby, Cellular Solids: Structure and Properties, Cambridge University Press, 1999.
[40] Y. Kwon, K. Thornton, P.W. Voorhees, Morphology and topology in coarsening of domains via non-conserved and conserved dynamics, Phil. Mag. 90 (1–4) (2010) 317–335.
[41] K.R. Mangipudi, E. Epler, C.A. Volkert, Topology-dependent scaling laws for the stiffness and strength of nanoporous gold, Acta Mater. 119 (2016) 115–122.
[42] K. Hu, M. Ziehmer, K. Wang, E.T. Lilleodden, Nanoporous gold: 3D structural analyses of representative volumes and their implications on scaling relations of mechanical behaviour, Phil. Mag. (2016) 1–14.
[43] R.E. Miller, V.B. Shenoy, Size-dependent elastic properties of nanosized structural elements, Nanotechnology 11 (3) (2000) 139–147.
[44] S. Mathesan, D. Mordehai, Size-dependent elastic modulus of nanoporous Au nanopillars, Acta Mater. 185 (2020) 441–452.
[45] B.A.M. Elsner, S. Müller, S. Bargmann, J. Weissmüller, Surface excess elasticity of gold: Ab initio coefficients and impact on the effective elastic response of nanowires, Acta Mater. 124 (2017) 468–477.
[46] C. Richert, A. Odermatt, N. Huber, Computation of thickness and mechanical properties of interconnected structures: Accuracy, deviations, and approaches for correction, Front. Mater. 6 (327) (2019).
[47] A. Hodge, R. Doucette, M. Biener, J. Biener, O. Cervantes, A. Hamza, Ag effects on the elastic modulus values of nanoporous Au foams, J. Mater. Res. 24 (4) (2009) 1600–1606.
[48] J. Biener, A.M. Hodge, A.V. Hamza, L.M. Hsiung, J.H. Satcher Jr., Nanoporous Au: A high yield strength material, J. Appl. Phys. 97 (2) (2005) 024301.
[49] M. Bürckert, N.J. Briot, T.J. Balk, Uniaxial compression testing of bulk nanoporous gold, Phil. Mag. 97 (15) (2017) 1157–1178.
[50] T.J. Balk, C. Eberl, Y. Sun, K.J. Hemker, D.S. Gianola, Tensile and compressive microspecimen testing of bulk nanoporous gold, JOM 61 (2009) 26–31.
[51] N. Badwe, X. Chen, K. Sieradzki, Mechanical properties of nanoporous gold in tension, Acta Mater. 129 (2017) 251–258.
[52] X.-Y. Sun, G.-K. Xu, X. Li, X.-Q. Feng, H. Gao, Mechanical properties and scaling laws of nanoporous gold, J. Appl. Phys. 113 (2) (2013) 023505.
[53] H. Jeon, N.-R. Kang, E.-J. Gwak, J.-i. Jang, H.N. Han, J.Y. Hwang, S. Lee, J.-Y. Kim, Self-similarity in the structure of coarsened nanoporous gold, Scr. Mater. 137 (2017) 46–49.
[54] Y. Li, B.-N.D. Ngô, J. Markmann, J. Weissmüller, Topology evolution during coarsening of nanoscale metal network structures, Phys. Rev. Mater. 3 (7) (2019) 076001.

[55] Y. Li, B.-N. Dinh Ngô, J. Markmann, J. Weissmüller, Datasets for the microstructure of nanoscale metal network structures and for its evolution during coarsening, Data Brief 29 (2020) 105030.
[56] A. Jacobsen, W. Barvosa-Carter, S. Nutt, Micro-scale truss structures formed from self-propagating photopolymer waveguides, Adv. Mater. 19 (22) (2007) 3892–3896.
[57] M. Kadic, T. Bückmann, N. Stenger, M. Thiel, M. Wegener, On the practicability of pentamode mechanical metamaterials, Appl. Phys. Lett. 100 (19) (2012) 191901.
[58] T. Tancogne-Dejean, A.B. Spierings, D. Mohr, Additively-manufactured metallic micro-lattice materials for high specific energy absorption under static and dynamic loading, Acta Mater. 116 (2016) 14–28.
[59] C. Richert, N. Huber, Skeletonization, geometrical analysis, and finite element modeling of nanoporous gold based on 3D tomography data, Metals 8 (4) (2018) 282.
[60] C. Richert, N. Huber, A comparison of ligament geometries in real and computer-generated nanoporous gold based on cross-section descriptors, Comput. Mater. Sci. 229 (2023) 112423.